Original Article

Conductivity mechanisms and influence of the Cu/Zn disorder on electronic properties of the powder Cu₂ZnSn(S₁₋ₓSeₓ)₄ solid solutions

Maxim Guc [a,c], Galina Gurieva [b], Elena Hajdeu-Chicarosh [a,*],
Susan Schorr [b,d], Konstantin G. Lisunov [a,e], Ernest Arushanov [a]

[a] Institute of Applied Physics, Academy of Sciences of Moldova, Academiei Str. 5, MD-2028, Chisinau, Republic of Moldova
[b] Helmholtz-Zentrum Berlin, Hahn-Meitner-Platz 1, 14109, Berlin, Germany
[c] Catalonia Institute for Energy Research (IREC), Jardins de Les Dones de Negre 1 2pl., Sant Adriàdel Besòs, Barcelona, 08930, Spain
[d] Freie Universitat Berlin, Malteserstr, 74-100, 12249, Berlin, Germany
[e] Department of Physics, Lappeenranta University of Technology, PO Box 20, FIN-53851, Lappeenranta, Finland

ABSTRACT

One of the major reasons for a recent stuck of the development of kesterite based photovoltaic devices is related to the problems in their open circuit voltage. Several limitations can be pointed out as a possible origin. In particular, for a case of Cu and Zn containing kesterite compounds, a lattice disorder connected to these cations is considered to bring in an important contribution to the limitations above. Extensive studies showed a significant influence of this disorder being an intrinsic property of kesterites to structural, optical and vibrational properties of the related materials. However, detailed investigations focused to the role of disorder in formation of the electrical properties of the kesterite materials are still lacking. In order to cover this gap, here is investigated resistivity of Cu₂ZnSn(S₁₋ₓSeₓ)₄ (CZTSSe) powder samples with $x = 0.48-1.00$ at temperatures between ~ 10 and 300 K. A detailed analysis of the measured data permits to establish various conductivity mechanisms within different temperature ranges, and to obtain a set of important macroscopic and microscopic electronic parameters. By itself, their dependence on x does not reveal any univocal behavior. In contrast, all the electronic parameters above exhibit a clear correlation with the order parameter Q. This is explained completely by a strong sensitivity of the electronic properties of CZTSSe to the Cu/Zn disorder.

1.   Introduction

The Cu$_2$ZnSnSe$_4$ (CZTS) and Cu$_2$ZnSn(S$_{1-x}$Se$_x$)$_4$ (CZTSSe) compound semiconductors are widely discussed now due to a possible application in photovoltaic and other optoelectronic devices [1–3]. Indeed, the efficiency up to 12.6% has been achieved in CZTSSe based solar cells [1]. At this point, such properties of CZTS and related materials as low cost, low toxicity, abundance of their elements in the crust, and a high flexibility of their physicochemical properties look probably no less attractive. However, several limitations existing in the kesterite type compounds have led to a current stagnation in the increase of the solar cell performance [4–6]. One of the most important out of them is connected to the influence of a disorder in a cation sublattice of the kesterite type structure. Namely, the Cu/Zn disordering was indicated as one of the limiting factors for further development of the kesterite based photovoltaic technology [7–9]. Structural properties [10,11], photoluminescence [10–12], Raman scattering [13,14] and transmittance [15] spectroscopies, as well as the absorption coefficient [12], have been discussed in this sense. These extensive investigations have revealed clear correlations between the Cu/Zn disordering and the properties of CZTSSe, mentioned above. However, any detailed studies of such influence on the electronic transport properties of CZTSSe are still lacking.

Generally, the electronic transport in CZTSSe and related materials is widely investigated, including single crystals [16–19], thin polycrystalline films [20–22] and powder samples [23,24]. One of its most characteristic features is the existence of a broad temperature interval with the Mott variable range hopping (VRH) conductivity [25,26]. However, manifestations and importance of this conduction mechanism in general depend substantially on the sample type (single crystals, powders or thin films), growing conditions and post-grown treatment [16–24]. Most commonly, the electronic transport is influenced by the chemical composition of the investigated material, namely the cations ratios Cu/(Zn + Sn) [27–30], Zn/Sn [27–29,31–33] and Cu/Sn [34], or even by a concentration of one of the cations [23,35]. On the other hand, the obtained picture still looks rather controversial in general (e.g. compare results of Refs. [32,33]), without evidence of any direct correlations in most of the cases reported [21,27]. A possible influence of the Cu/Zn disorder on the electrical properties of CZTSSe has been proposed [27,36]. However, such infer looks rather preliminary, containing no deeper analysis of the results and absence of any quantitative data characterizing the disorder.

In this context, in the present work detailed investigations of the resistivity in CZTSSe powder samples within a broad range of composition and temperature have been performed. A choice of the powder sample was connected with their high structural and compositional uniformity and with a possibility to perform an independent direct investigation of their order parameter by a neutron diffraction study [11]. A combined analysis of these results with those of the resistivity above have been done. This permitted to obtain an important set of macroscopic and microscopic electronic parameters, yielding a reliable information about a strong influence of the cation disorder on the electronic properties of CZTSSe.

2.   Experimental details

The samples were grown by solid–state reaction; detailed analysis of their structural, vibrational and irradiative properties has been published elsewhere [11]. The phase content and chemical composition of the synthesized polycrystalline powder samples were measured by wavelength dispersive X-ray spectroscopy (WDX), using an electron microprobe system (JEOL-JXA 8200). Grains, identified to belong to the same phase (i.e. with the same amounts of Cu and/or Zn and/or Sn and/or S within the error of the WDX measurement), were averaged. As has been found from these data, the values of the Cu/(Zn + Sn) and Zn/Sn ratios are equal to unity for all samples, whereas the Se/(Se + S) ratio or x varies within the range of $x = 0.48-1.00$ with a step of ~0.1 [11]. Besides the anions ratio above, the variation of the degree of disorder has been found in the investigated samples. The disorder is characterized by the order parameter Q (see Table 1), which can be defined via the site occupation factors of 2c and 2d sites by the Cu and Zn atoms, respectively [10], in the kesterite type structure,

$$Q = \frac{[Cu_{2c} + Zn_{2d}] - [Zn_{2c} + Cu_{2d}]}{[Cu_{2c} + Zn_{2d}] + [Zn_{2c} + Cu_{2d}]}. \tag{1}$$

The site occupation factors have been determined by neutron diffraction investigations (the details can be found in Refs. [10,11]). Note, that the parameter Q is defined with Eq. (1) in such a way that $Q = 0$ for a complete disorder and $Q = 1$ for a complete order. However, in what follows, a conjugate order parameter, $Q' = 1 - Q$, will be widely used for convenience.

The hot probe method, addressed to the thermopower measurements, showed the p-type conductivity in all

Table 1 – Anionic ratio and order parameter of the analyzed CZTSSe powder sample, together with temperature intervals, width of the acceptor band and activation energies of the observed conductivity mechanisms.

x	Q	Q'	ΔT_v (K)	T_0 (10^3 K)	W (meV)	ΔT_n (K)	E_n (meV)	ΔT_a (K)	E_a (meV)
0.48	0.38	0.62	55–125	13.10	17.3	120–165	19.0	12–16	0.22
0.58	0.2	0.8	45–100	66.80	21.7	140–180	26.7	11–17	0.59
0.70	0.14	0.86	65–125	44.90	23.3	150–185	27.0	15–19	0.71
0.79	0.5	0.5	55–90	3.00	12.3	95–115	11.8	13–17	0.12
0.90	0.6	0.4	30–70	0.29	4.4	40–80	5.4	12–16	0.02
1.00	0.4	0.6	30–90	7.36	11.7	85–115	13.3	11–14	0.29

samples, as typical of the whole family of Cu based kesterite type compounds. The temperature dependence of the resistivity was investigated with the Van der Pauw method. For these purpose, CZTSSe powder samples were pressed into pellets with a diameter of 5 mm and a thickness of ~2–3 mm. Silver paste was used to produce the contacts. The CZTSSe pellet was placed in a closed circle helium cryostat to vary the temperature between $T = 10–300$ K.
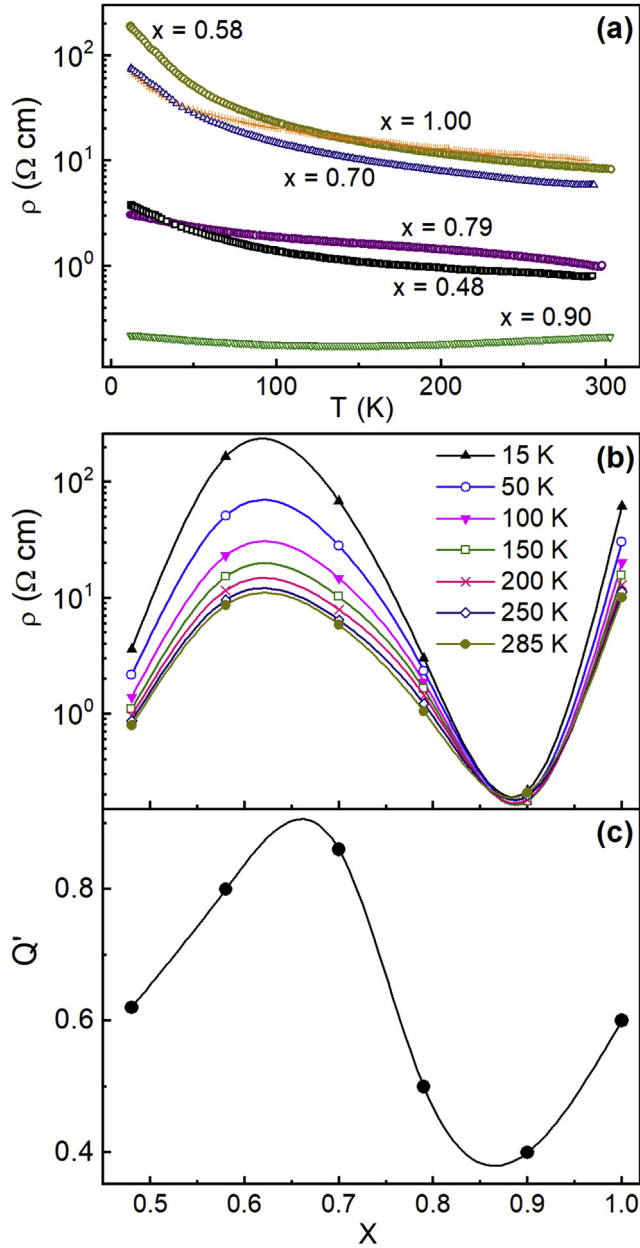

Fig. 1 – (a) Temperature dependence of the resistivity for different x. (b) Dependence of the resistivity on the compositional value x for different temperatures. (c) Plots of Q′ vs. x. The lines are the spline interpolation of the data points.
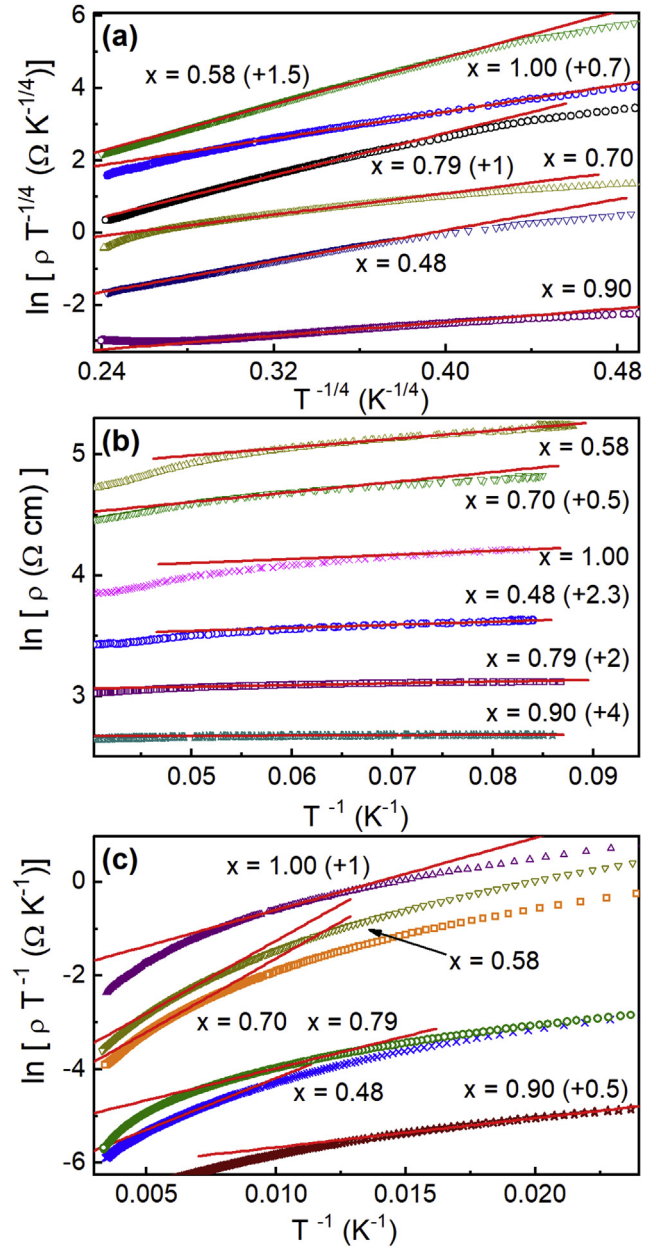

Fig. 2 – Plots of $\ln(\rho T^{-1/4})$ vs. $T^{-1/4}$(a), of $\ln(\rho)$ vs. T^{-1} (b) and of $\ln(\rho T^{-1})$ vs. T^{-1}(c). The lines are linear fits. For convenience, some data are shifted along the vertical axes by the values in parenthesis.

3. Results and discussion

3.1. Experimental results

As can be seen in Fig. 1a, the majority of samples exhibit an activated dependence of $\rho(T)$ within the whole temperature range. The only exclusion is observed at $x = 0.9$, where such dependence takes place only below $T = 150$ K. The different strength of $\rho(T)$ with decreasing temperature is attributable to

different proximity of the samples to the metal-insulator transition (MIT), what has been often observed in kesterites and related materials with different morphological state [16−19,21,24]. On the other hand, the dependence of $\rho(x)$ is quite unusual, being essentially non-linear at any T, including a maximum near $x_{max} \approx 0.6$ and a minimum close to $x_{min} \approx 0.9$ (Fig. 1b). However, such behavior of $\rho(x)$ following approximately that of $Q'(x)$, shown in Fig. 1c, is quite in line with the strong sensitivity of the resistivity to the degree of the cation disorder. This has been assumed earlier in $Cu_2ZnSn_{x-}Ge_{1-x}Se_4$ (CZTGeSe) solid solutions [19]. It can be seen, that the shape of the $\rho(x)$ curves in Fig. 1 do not follow that of the order parameter explicitly. However, one should keep in mind the macroscopic nature of the resistivity, containing various random factors (depending in particular on preparation details), which are difficult to take into account precisely. However, such factors are expected to have a smaller influence on the microscopic electronic parameters of the materials, which suggests a further analysis of the resistivity and will be evident below.

3.2. Macroscopic behavior of $\rho(T)$

As mentioned in the introduction, the Mott VRH conduction is common for many kesterite type and related materials, taking place within a broad temperature range, irrespective of the macroscopic sample state. The resistivity for this mechanism is given by the expression

$$\rho(T) = DT^{1/4} \exp\left[(T_0/T)^{1/4}\right], \qquad (2)$$

where D is the VRH prefactor coefficient, and

$$T_0 = \beta / \left[k_B g(\mu)a^3\right] \qquad (3)$$

is the VRH characteristic temperature, $\beta = 21$ is the numerical constant, $g(\mu)$ is the density of the localized states (DOS) at the Fermi level, μ, and a is the localization radius of charge carriers, scaling the space decay of the impurity wave functions [25,37].

As can be seen in Fig. 2a, all the exhibited plots have broad linear intervals, pertinent to the Mott VRH conduction according to Eq. (2). With a linear fit of the measured resistivity data, the values of T_0, along with the temperature intervals, ΔT_v, of the Mott VRH conduction, were obtained (see Table 1). In addition, the width of the acceptor band (AB) W has been found with the expression $W \approx 0.5 k_B (T_{v3} T_0)^{1/4}$ [16,17,37], where T_v is the Mott VRH onset temperature on cooling (the left value of the intervals ΔT_v in Table 1), and is collected in Table 1, too. The obtained here values of W are comparable with those of ~11−37 meV reported for Cu_2ZnSnS_4 (CZTS) single crystals and as-grown thin films [16,18,21], but significantly smaller than those of ~90−174 meV obtained for CZTS powder-samples [24] and thermal treated thin films [21]. This can be related to an increased cationic disorder in the latter, as well as to presence of significant amount of point defects due to the off-stoichiometric composition of these samples.

On the other hand, the nearest-neighbor hopping (NNH) conductivity mechanism, given by the law

$$\rho(T) = CT^{-1} \exp\left[E_n / (k_B T)\right], \qquad (4)$$

where C is the NNH prefactor constant and E_n is the NNH activation temperature, is expected within a temperature interval ΔT_n lying generally above ΔT_v, provided that $E_n \sim W$ [37]. This has been already observed in CZTS and CZTGeSe single crystals [16,18,19]. At this point, one can choose intervals ΔT_n of linearization of the resistivity data plots in Fig. 2c to satisfy both the conditions above. Indeed, this can be seen by comparing the data of ΔT_n and E_n, collected in Table 1, with those of ΔT_v and W, respectively. The only exception is for CZTSSe with $x = 0.9$, where the intervals of ΔT_n and ΔT_v are overlapped. This is not too surprising due to a quite week temperature dependence of the resistivity for this sample in general.

The last conduction mechanism out of those analyzed here is convenient to discuss after formulating the AB DOS model, which is given in Fig. 3. It is considered to be of the Anderson type [25], centered at $E_A = 0$ (where E_A is the acceptor activation energy) and is characterized by a finite total width of 2W. The parameters $-E_c$ and E_c in Fig. 3 are the mobility edges, separating the delocalized acceptor states from the localized states (which are hatched), and E_v is the edge of the valence band. The activated behavior of $\rho(T)$ above (see Fig. 1) corresponds to a position of μ inside one out of the intervals of localized states, whereas MIT takes place when μ passes through $-E_c$ or E_c [25]. Therefore, different strength of $\rho(T)$ in the activated interval, associated with different closeness to the MIT above, is given by the various distances between μ and one of the mobility edges, $E_a = |\mu - E_c|$.

The actual position of μ in Fig. 3 corresponds to a strong degree of compensation, $K = N'/N$, where N' and N are the concentrations of donors and acceptors, respectively. In such a situation, one can expect the existence of a temperature interval ΔT_a, where the conductivity, connected to a thermal activation of charge carriers from μ to the energy interval $(-E_c,$
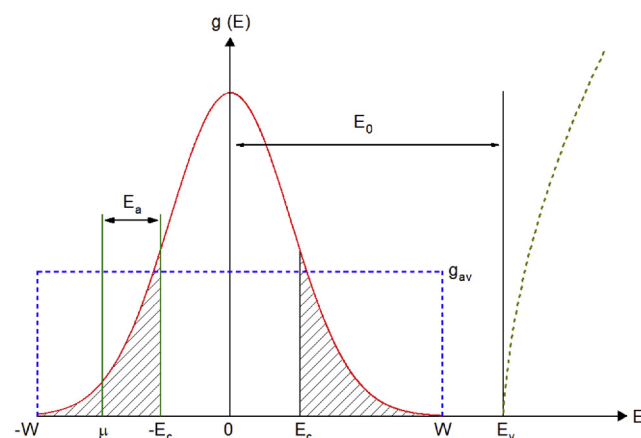

Fig. 3 — Image of the DOS vs. energy with width 2W in the acceptor band (schematically, not in scale). The extended states lie between the mobility edges $-E_c$ and E_c, the localized states are hatched (solid line). The dotted line represents the approximation of the DOS with the rectangular shape, given by the average DOS $g_{av} = N/(2W)$. The dashed line is the DOS in the valence band and E_v is its edge.

E_c), should dominate. The resistivity for such a mechanism is given by the expression

$$\rho(T) = \rho_0 \exp[E_a / (k_B T)], \tag{5}$$

where ρ_0 is the prefactor constant [25]. The particularity of this conductivity mechanism consists in the fact that the temperature ranges in which it is realized, ΔT_a, can lie at temperatures higher or lower than ΔT_v, depending on energetic distance between μ and $-E_c$ [38]. The mechanism above has been already observed in $Cu_2ZnSiSe_4$ [17] single crystals and CZTS powder samples [24] at temperatures ΔT_a ~200—300 K lying above ΔT_v, as well as in Cu_2ZnGeS_4 single crystals both at temperatures higher and lower than ΔT_v [38]. This is in line with the strong degree of compensation in these materials. The existence of a third charge transfer mechanism, or the intervals ΔT_a above, can be verified in our case after the determination of the parameters μ and E_c in our samples, assuming the strong compensation and the position of μ as shown in Fig. 3.

3.3. Determination of microscopic parameters

To simplify the problem, we apply a rectangular DOS approximation, given in Fig. 3 by the dotted line, where $g_{av} = N/(2W)$ is the average DOS value, which will be used instead of the explicit one or $g(E)$. Such approximation has been reasonably utilized in the analysis of $\rho(T)$ in kesterites [16—18,21], although it can provide another source of errors, what has been discussed in [16,17].

The general expression of the localization radius can be given in the form:

$$a = a_B(1 - N/N_C)^{-\nu}, \tag{6}$$

where $\nu \approx 1$ is the critical exponent of the correlation length, $a_B = \hbar^2 \kappa_0/(m e^2)$ is the Bohr radius, m is the hole effective mass, κ_0 is the dielectric permittivity far from the MIT and N_C is the critical acceptor concentration of the MIT [25,26,37,39]. The latter is connected to a_B with the universal Mott criterion, $N_C^{1/3} a_B \approx 0.25$ [25,26,39]. Combining this criterion with Eq. (3) at $g(\mu) = g_{av}$ and Eq. (6), one can find the expression

$$\left(\frac{T_0}{T_v}\right)^{1/4} \approx 4\beta^{1/3} \left(\frac{N_C}{N}\right)^{1/3} \left(1 - \frac{N}{N_C}\right)^\nu, \tag{7}$$

yielding the values of N/N_C and those of a/a_B (see Table 2). For the next step, according to Ref. [25], another expression of a, conformed with the energy scale of Fig. 3, can be written as

$$a = a_B \left(1 - \frac{W + \mu}{W + E_c}\right)^{-\nu}, \tag{8}$$

where

$$E_c = -W + V_0^2 / [4(z - 1)J]. \tag{9}$$

Here, $V_0 \approx 2W$ is the typical width of the carrier potential energy, expanded due to disorder, $z = 6$ is the coordination number and $J = J_0 \exp(-R/a_B)$ is the overlap integral [25]. The parameter $R = (4\pi N_A/3)^{-1/3}$ describes the half of the mean distance between acceptors, whereas the prefactor J_0 for the case of a broad impurity (acceptor) band can be expressed as [17,25].

$$J_0 = \frac{e^2}{\kappa_0 a_B} \left[\frac{3}{2}\left(1 + \frac{R}{a_B}\right) + \frac{1}{6}\left(\frac{R}{a_B}\right)^2\right]. \tag{10}$$

In the calculations we apply a linear approximation of the hole effective mass, $m(x) = 0.49(1 - x) + 0.23x$, where the values of $m = 0.49$ and 0.23 (in units of the free electron mass) are addressed to the mean hole effective mass in the end members of the CZTSSe solid solution, which are CZTS and CZTSe [40,41]. In addition, here we use the same approximation of the band gap energy, $E_g(x) = 1.5(1 - x) + 0.8x$ (in eV) [41]. Finally, with the results of Ref. [42] one can obtain the relation $\kappa_0(x) = 7.0 + 1.9x$ within the linear approximation, too. The calculated values of a_B and N_C are collected in Table 2. The values of a and N_A are evaluated with those of N/N_C, a_B and N_C in Table 2, yielding in turn those of g_{av} (see Table 2) obtained with the corresponding data of W in Table 1. Finally, the values of μ and E_c are calculated with Eq. (8—10) by variation of μ at any x to reproduce explicitly the values for a above with Eq. (8). The values of μ, E_c and $E_a^{(cal)} = |\mu - E_c|$ are collected in Table 2. All the obtained values agree reasonably with those observed earlier in other related kesterites [16—19,21,24], depending on proximity to the MIT and on the cationic disorder.

3.4. Identification of the third (low-temperature) conduction mechanism

As can be seen in Table 2, all the calculated values of $E_a^{(cal)}$ correspond to an interval ΔT_a at low temperatures (LT) lying definitely below the Mott conduction or ΔT_v. Hence, those of ΔT_a have been searched by linearization of the plots in the middle panel of Fig. 2 according to Eq. (5) at $T < 30$ K. The data of ΔT_a and the experimental values of E_a, obtained with linear fits of the plots in the middle panel of Fig. 2, are collected in Table 1. For convenience, the data of E_a are reproduced in

Table 2 — Microscopic electronic parameters of CZTSSe powder samples.

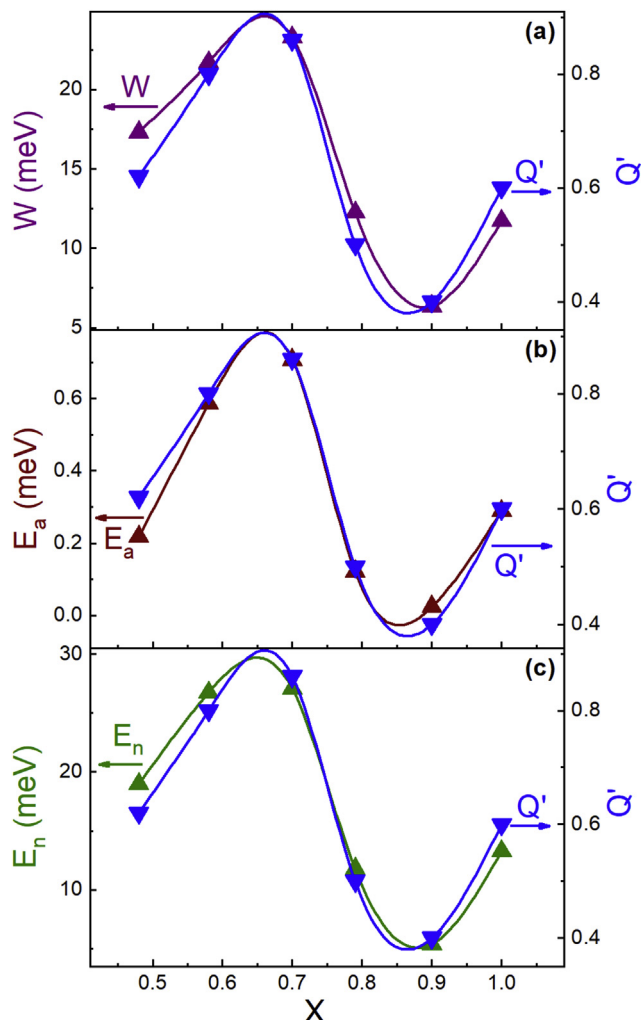| x	a_B (Å)	N_C (10^{18} cm^{-3})	a/a_B	N/N_C	g_{av} (10^{17} cm^{-3} meV^{-1})	$-E_c$ (meV)	$-\mu$ (meV)	$E_a^{(cal)}$ (meV)	E_a (meV)
0.48	11.7	9.70	3.8	0.74	2.07	16.5	16.7	0.22	0.22
0.58	13.1	6.96	2.6	0.61	0.98	20.0	20.7	0.65	0.59
0.70	14.3	5.38	2.9	0.66	0.76	21.2	21.9	0.72	0.71
0.79	16.2	3.71	5.4	0.81	1.23	11.6	11.7	0.12	0.12
0.90	17.8	2.78	8.2	0.88	2.75	4.3	4.3	0.01	0.02
1.00	20.5	1.80	4.0	0.75	0.58	10.7	11.0	0.25	0.29

Fig. 4 − Plots of W vs. x (a), of E_a vs. x (b) and of E_n vs. x (c), displayed along with the plots of Q′ vs. x. The lines are the spline interpolation of the data points.

data sets is evident, which is in a complete agreement to the different proximity of the samples to the MIT at different x values, as has been supposed preliminary in Section 3.1. In particular, the highest values of a/a_B and N/N_C for CZTSSe x = 0.9 (Table 2) indicate the most closeness of this sample to the MIT. At the same time, the weakest dependence of $\rho(T)$ for this sample suggests just the same situation. Similar inference can be drawn with the data of E_c and μ (Table 2), both lying quite close to the AB edge (cf. them with the data of W in Table 1), and especially with the values of $E_a^{(cal)}$ in Table 2.

On the other hand, all the electronic parameters, which determine the charge transfer mechanisms (collected in Tables 1 and 2), are quite sensitive to the degree of the microscopic structural disorder in general. This has been already observed for different kesterite type and related materials, but only indirectly, without specification of the disorder type and details [17−19,21]. Here, we concentrate on the direct evidence for different important parameters, depending on the degree of the cation disorder, based on direct independent determinations of the order parameter in the same samples [11]. For this purpose, we plot the dependences of W, E_a and E_n versus x along with that of Q′ on x. As can be seen in Fig. 4, all the data above are reproduced with the Q′(x) curves in detail. This is demonstrated alternatively in Fig. 5, where the dependencies of W, E_n and E_a on Q′ are close to linear. Some deviations of the shape of the corresponding curves from that of Q′(x) in Fig. 4 and from the linearity in Fig. 5 are attributable to a small additional disorder, induced by the variation of the S/(S + Se) ratio, as well as some random uncontrolled factors above. At the same time, one can see that the correlations between the data of W, E_n and E_a with those of Q′ are much better, than the corresponding behavior in Fig. 1a and c. This is not surprising, taking into account a smaller influence of the random factors on the microscopic parameters with respect to that of the macroscopic parameters such as the resistivity.

Finally, in the frame of the general scheme above, we plot the reciprocal values of some electronic parameters in Table 2 along with the dependence of Q′(x), as shown in Fig. 6. Clear correlations between the curves of N_C/N and a/a_B vs. x with
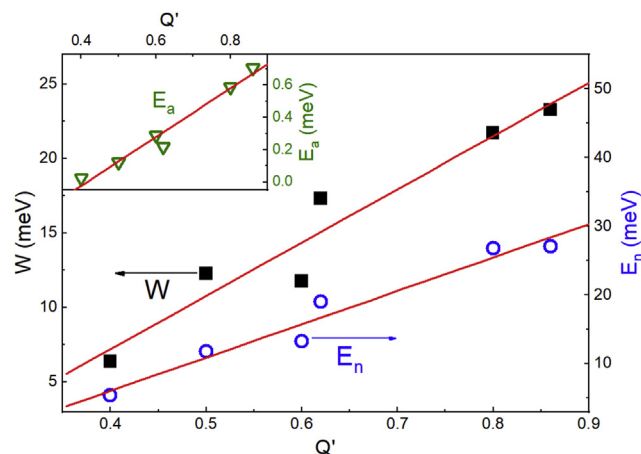
Table 2, too, near the calculated values of $E_a^{(cal)}$. One can see a reasonable agreement between E_a and $E_a^{(cal)}$. This supports the strong compensation in the CZTSSe samples and the existence of the LT charge transfer mechanism, connected to the activation of the holes on the mobility threshold according to Eq. (5). The result for the case of CZTSSe with x = 0.9, where both parameters are only comparable, indicates probably an insufficient accuracy of our calculations under the rectangular approximation for this case, where the dependence of $\rho(T)$ is too weak (Fig. 1). Indeed, the values of E_a and $E_a^{(cal)}$ themselves for x = 0.9 are practically on the order of the error or difference between the corresponding data for the rest of samples.

3.5.   Discussion (role of disorder)

First of all, one should mention the values of a/a_B and N/N_C in Table 2 in the context of the strength of the activated $\rho(T)$ behavior (see Fig. 1a). Indeed, a clear correlation of the both

Fig. 5 − The dependencies of W and E_n on Q′. Inset: Plot of E_a vs. Q′. The lines are linear fits.
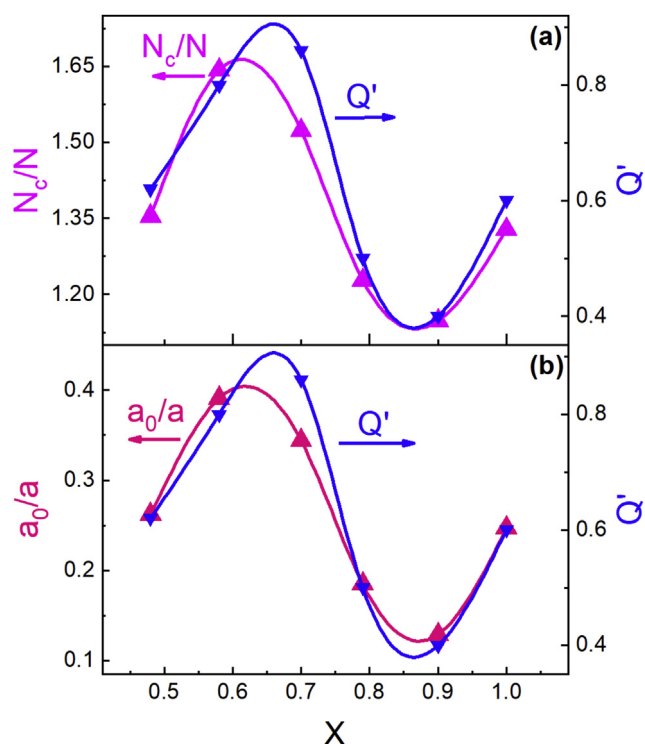
Fig. 6 – Plots of N_C/N (a) and of a_B/a vs. x (b), displayed along with the plots of Q' vs. x. The lines are the spline interpolation of the data points.

that of $Q'(x)$ are evident, too, although somewhat less explicit than those in Fig. 4. However, one should keep in mind that the corresponding data in Fig. 6 have been obtained within a less direct way, than those in Figs. 4 and 5. In particular, the former contain some additional error, connected to a rectangular approximation of an unknown DOS shape (in Fig. 3). Nevertheless, a strong direct influence of the cation disorder on the microscopic electronic parameters of the CZTSSe compounds can be deduced from Fig. 6, too, which is in line with the results discussed above.

It is worth to mention, that selected uniform powder samples had cations ratios close to unity, as mentioned in Section 2. In addition, no or insignificant amount of additional point defects were found in the investigated samples, as has been established by the neutron diffraction analysis [11]. The data of the conductivity mechanisms and of the electronic parameters found here can be compared with those published previously for different kesterite type compounds (including different elemental compositions [27—35] and morphological states [16—24]). In this way, one can establish an insignificant dependence of the general behavior of the resistivity in these materials on the cations ratio, including even a partial or complete replacement of Sn. This permits to infer, that the Cu/Zn disorder is probably a main reason, which contributes to the formation of the acceptor band. In turn, this leads to observation of a rather complicated conductivity mechanism, related to the hopping of the charge carriers already up to the

room temperature, in the kesterite type materials. In this respect, detailed investigations of the electronic transport in the quaternary compounds from the same family but with the partial or complete replacement of Cu or Zn cations may be recommended in order to reach a deeper insight of the role and details of the cation disorder in these materials.

4. Summary and conclusions

The resistivity of the $Cu_2ZnSn(S_{1-x}Se_x)_4$ solid solution (powder samples) in a wide temperature range has been investigated. The analysis of $\rho(T)$ has permitted to determine the charge transfer mechanisms in CZTSSe within different temperature intervals, including the high-temperature nearest neighbor hopping conductivity, followed by the Mott variable-range hopping with lowering T and, eventually, by the activation of the holes on the mobility edge of the acceptor band at lowest temperatures. The characteristic resistivity parameters for all the mechanisms above have been determined. In turn, their further analysis has yielded important microscopic parameter, such as the localization radius and the acceptor concentration, as well as some details of the hole spectrum in the acceptor band. These include the bandwidth and positions of the Fermi energy as well as the mobility threshold. A special attention has been paid to the influence of the cation disorder on the electronic properties of the material. Namely, the observed quite unusual dependence of $\rho(x)$ has been interpreted by a similar shape of the conjugate order parameter $Q'(x)$. In addition, even a more dramatic role of the cation disorder in CZTSSe has been established by the observation of direct correlations between the order parameter and the microscopic electronic parameters, obtained by the analysis of $\rho(T)$ data. To summarize, a direct evidence of the influence of the cation disorder on the electronic properties of CZTSSe has been established. Moreover, the high compositional uniformity and absence of additional point defects in the analyzed samples should be underlined. The comparison with the previously published results on detailed investigation of electrical properties of kesterite type compounds is important at this point, too. The items above permit to infer, that namely the disorder in the Cu/Zn substructure is probably a decisive factor, which is responsible for appearance of the acceptor band and the observed complicated charge transfer mechanism in these materials.

Declaration of Competing Interest

The authors declare that they have no known competing financial interests or personal relationships that could have appeared to influence the work reported in this paper.

Acknowledgements

REFERENCES

[1] Wang W, Winkler MT, Gunawan O, Gokmen T, Todorov TK, Zhu Y, et al. Device characteristics of CZTSSe thin-film solar cells with 12.6% efficiency. Adv Energy Mater 2014;4:1301465. https://doi.org/10.1002/aenm.201301465.

[2] Liu M-L, Huang Fu-Q, Chen Li-D, Chen I-W. A wide-band-gap p-type thermoelectric material based on quaternary chalcogenides of Cu_2ZnSnQ_4 (Q = S, Se). Appl Phys Lett 2009;94:202103. https://doi.org/10.1063/1.3130718.

[3] Tsuji I, Shimodaira Y, Kato H, Kobayashi H, Kudo A. Novel stannite-type complex sulfide photocatalysts A^I_2-Zn-A^{IV}-S4 (A^I = Cu and Ag; A^{IV} = Sn and Ge) for hydrogen evolution under visible-light irradiation. J Mater Chem 2010;22:1402–9. https://doi.org/10.1021/cm9022024.

[4] Sardashti K, Haight R, Gokmen T, Wang W, Chang L-Y, Mitzi DB, et al. Impact of nanoscale elemental distribution in high-performance kesterite solar cells. Adv Energy Mater 2015;5:1402180. https://doi.org/10.1002/aenm.201402180.

[5] Giraldo S, Jehl Z, Placidi M, Izquierdo-Roca V, Pérez-Rodríguez A, Saucedo E. Progress and perspectives of thin film kesterite photovoltaic technology: a critical review. Adv Mater 2019;31:1806692. https://doi.org/10.1002/adma.201806692.

[6] Fonoll-Rubio R., Andrade-Arvizu J., Blanco-Portals J., Becerril-Romero I., Guc M., Saucedo E., et al. Insights into interface and bulk defects in a high efficiency kesterite-based device, Energy Environ Sci/In press/.

[7] Gokmen T, Gunawan O, Todorov TK, Mitzi DB. Band tailing and efficiency limitation in kesterite solar cells, Appl. Phys Lett 2013;103:103506. https://doi.org/10.1063/1.4820250.

[8] Scragg JJS, Larsen JK, Kumar M, Persson C, Sendler J, Siebentritt S, et al. Cu–Zn disorder and band gap fluctuations in $Cu_2ZnSn(S,Se)_4$: theoretical and experimental investigations. Phys Status Solidi B 2016;253:247–54. https://doi.org/10.1002/pssb.201552530.

[9] Bourdais S, Choné C, Delatouche B, Jacob A, Larramona G, Moisan C, et al. Is the Cu/Zn disorder the main culprit for the voltage deficit in kesterite solar cells? Adv Energy Mater 2016;6:1502276. https://doi.org/10.1002/aenm.201502276.

[10] Tobbens DM, Gurieva G, Levcenko S, Unold T, Schorr S. Temperature dependency of Cu/Zn ordering in CZTSe kesterites determined by anomalous diffraction. Phys Status Solidi B 2016;253:1890–7. https://doi.org/10.1002/pssb.201600372.

[11] Gurieva G, Többens DM, Levcenco S, Unold T, Schorr S. Cu/Zn disorder in stoichiometric $Cu_2ZnSn(S_{1-x}Se_x)_4$ semiconductors: a complimentary neutron and anomalous X-ray diffraction study. J Alloys Compd 2020;846:156304. https://doi.org/10.1016/j.jallcom.2020.156304.

[12] Valentini M, Malerba C, Menchini F, Tedeschi D, Polimeni A, Capizzi M, et al. Effect of the order-disorder transition on the optical properties of Cu_2ZnSnS_4. Appl Phys Lett 2016;108:211909. https://doi.org/10.1063/1.4952973.

[13] Scragg JJS, Choubrac L, Lafond A, Ericson T, Platzer-Bjorkman C. A low-temperature order-disorder transition in Cu_2ZnSnS_4 thin films. Appl Phys Lett 2014;104:041911. https://doi.org/10.1063/1.4863685.

[14] Dimitrievska M, Giraldo S, Pistor P, Saucedo E, Pérez-Rodríguez A, Izquierdo-Roca V. Raman scattering analysis of the surface chemistry of kesterites: impact of post-deposition annealing and Cu/Zn reordering on solar cell performance. Sol Energy Mater Sol Cell 2016;157:462–7. https://doi.org/10.1016/j.solmat.2016.07.009.

[15] Stroth C, Sayed MH, Neerken J, Mikolajczak U, Rey G, Parisi J, et al. In-situ investigation of the order-disorder transition in $Cu_2ZnSnSe_4$ by optical transmission spectroscopy. AIP Adv 2017;7:025303. https://doi.org/10.1063/1.4976619.

[16] Lisunov KG, Guk M, Nateprov A, Levcenko S, Tezlevan V, Arushanov E. Features of the acceptor band and properties of localized carriers from studies of the variable-range hopping conduction in single crystals of p-Cu2ZnSnS4. Sol Energy Mater Sol Cell 2013;112:127–33. https://doi.org/10.1016/j.solmat.2013.01.027.

[17] Lisunov KG, Guc M, Levcenko S, Dumcenco D, Huang YS, Gurieva G, et al. Energy spectrum of near-edge holes and conduction mechanisms in Cu2ZnSiSe4 single crystals. J Alloys Compd 2013;580:481–6. https://doi.org/10.1016/j.jallcom.2013.06.156.

[18] Lähderanta E, Guc M, Shakhov MA, Arushanov E, Lisunov KG. Influence of scattering and interference effects on the low-temperature magnetotransport of Cu2ZnSnS4 single crystals. J Appl Phys 2016;120:035704. https://doi.org/10.1063/1.4959107.

[19] Lähderanta E, Hajdeu-Chicarosh E, Shakhov MA, Guc M, Bodnar IV, Arushanov E, et al. Hopping magnetotransport of the band-gap tuning $Cu_2Zn(Sn_xGe_{1-x})Se_4$ crystals. J Phys Condens Mat 2016;28:455801. https://doi.org/10.1088/0953-8984/28/45/455801.

[20] Guc M, Espíndola Rodríguez M, Bruc LI, Lisunov KG, Dermenji L, Curmei N, et al. In: Proceedings of 28th European photovoltaic solar energy conference and exhibition, Paris, France; 2013. p. 2449.

[21] Guc M, Caballero R, Lisunov KG, López N, Arushanov E, Merino JM, et al. Disorder and variable-range hopping conductivity in Cu_2ZnSnS_4 thin films prepared by flash evaporation and post-thermal treatment. J Alloys Compd 2014;596:140–4. https://doi.org/10.1016/j.jallcom.2014.01.177.

[22] Dermenji L, Guc M, Bruc LI, Dittrich Th, Rusu M, Lisunov KG, et al. In: Proceedings of 29th European photovoltaic solar energy conference and exhibition, Amsterdam, Netherlands; 2014. p. 1801.

[23] Hazama H, Tajima S, Masuoka Y, Asahi R. Transport properties of the Cu_2ZnSnS_4 bulk systems: effects of non-stoichiometry and defect formation. J Alloys Compnds 2016;657:179–83. https://doi.org/10.1016/j.jallcom.2015.10.032.

[24] Hajdeu-Chicarosh E, Guc M, Lisunov KG, Neldner K, Gurieva G, Schorr S, et al. Mechanisms of conductivity and energy spectrum of near-edge holes in Cu_2ZnSnS_4 powder samples. J Alloys Compd 2017;703:315–20. https://doi.org/10.1016/j.jallcom.2017.01.352.

[25] Mott NF, Davies EA. Electron processes in non-crystalline materials. Oxford: Clarendon; 1979.

[26] Mott NF. Metal–insulator transitions. London: Taylor and Francis; 1990.

[27] Kosyak V, Karmarkar MA, Scarpulla MA. Temperature dependent conductivity of polycrystalline Cu_2ZnSnS_4 thin films. Appl Phys Lett 2012;100:263903. https://doi.org/10.1063/1.4731875.

[28] Tanaka T, Yoshida A, Saiki D, Saito K, Guo Q, Nishio M, et al. Influence of composition ratio on properties of Cu_2ZnSnS_4 thin films fabricated by co-evaporation. Thin Solid Films 2010;518:S29–33. https://doi.org/10.1016/j.tsf.2010.03.026.

[29] Nagaoka A, Miyake H, Taniyama T, Kakimoto K, Yoshino K. Correlation between intrinsic defects and electrical properties in the high-quality Cu_2ZnSnS_4 single crystal. Appl Phys Lett 2013;103:112107. https://doi.org/10.1063/1.4821279.

[30] Bishop DM, McCandless BE, Haight R, Mitzi DB, Birkmire RW. Fabrication and electronic properties of CZTSe single crystals. IEEE J Photovoltaics 2015;5:390–4. https://doi.org/10.1109/JPHOTOV.2014.2363552.

[31] Tsega M, Kuo D-H. Defects and its effects on properties of Cu-deficient $Cu_2ZnSnSe_4$ bulks with different Zn/Sn ratios. APEX 2012;5:091201. https://doi.org/10.1143/APEX.5.091201.

[32] Ansari MZ, Khare N. Thermally activated band conduction and variable range hopping conduction in Cu_2ZnSnS_4 thin films. J Appl Phys 2015;117:025706. https://doi.org/10.1063/1.4905673.

[33] González JC, Fernandes PA, Ribeiro GM, Abelenda A, Viana ER, Salomé PMP, et al. Influence of the sulphurization time on the morphological, chemical, structural and electrical properties of Cu_2ZnSnS_4 polycrystalline thin films. Sol Energy Mater Sol Cell 2014;123:58–64. https://doi.org/10.1016/j.solmat.2014.01.005.

[34] García-Hemme E, Fairbrother A, Calvo-Barrio L, Saucedo E, Martil I. Compositional dependence of chemical and electrical properties in Cu_2ZnSnS_4 thin films. IEEE J Photovoltaics 2016;6:990–6. https://doi.org/10.1109/JPHOTOV.2016.2566888.

[35] Kuo D-H, Wubet W. Improvements in electrical properties for the Sn-rich $Cu_{2-x}ZnSnSe_4$ bulks with mobility above 50 cm^2/V

s. J Alloys Compd 2014;614:75–9. https://doi.org/10.1016/j.jallcom.2014.06.070.

[36] Bishop DM, McCandless B, Gershon T, Lloyd MA, Haight R, Birkmire R. Modification of defects and potential fluctuations in slow-cooled and quenched $Cu_2ZnSnSe_4$ single crystals. J Appl Phys 2017;121:065704. https://doi.org/10.1063/1.4975483.

[37] Shklovskii BI, Efros AL. Electronic properties of doped semiconductors. Berlin: Springer; 1984.

[38] Guc M, Lähderanta E, Hajdeu-Chicarosh E, Levcenko S, Shakhov MA, Zakharchuk I, et al. Mechanisms of charge transfer and electronic properties of Cu_2ZnGeS_4 from investigations of the high-field magnetotransport. Sci Rep 2017;7:10685. https://doi.org/10.1038/s41598-017-10883-0.

[39] Castner TG. Hopping conduction in the critical regime approaching the metal-insulator transition. In: Pollak M, Shklovskii B, editors. Hopping transport in solids. Amsterdam: North-Holland; 1991. p. 1–47. https://doi.org/10.1016/B978-0-444-88037-6.50007-5.

[40] Persson C. Electronic and optical properties of Cu_2ZnSnS_4 and $Cu_2ZnSnSe_4$. J Appl Phys 2010;107:053710. https://doi.org/10.1063/1.3318468.

[41] Liu H-R, Chen S, Zhai Y-T, Xiang HJ, Gong XG, Wei Su-H. First-principles study on the effective masses of zinc-blend-derived Cu_2Zn-IV-VI_4 (IV = Sn, Ge, Si and VI = S, Se). J Appl Phys 2012;112:093717. https://doi.org/10.1063/1.4759322.

[42] Gunawan O, Gokmen T, Warren CW, Cohen JD, Todorov TK, Aaron D, et al. Electronic properties of the $Cu_2ZnSn(Se,S)_4$ absorber layer in solar cells as revealed by admittance spectroscopy and related methods. Appl Phys Lett 2012;100:253905. https://doi.org/10.1063/1.4729751.